

Proceedings of the ASME 2024 Conference on Smart Materials,
Adaptive Structures and Intelligent Systems
SMASIS2024
September 9-11, 2024, Atlanta, Georgia

SMASIS2024-141593

PROGRAMMING OF NONLINEAR HETEROGENEOUS METAMATERIAL FOR SHOCK AND VIBRATION

Qianyu Zhao

School of Mechanical Engineering and Ray W. Herrick Laboratories Purdue University West Lafayette, Indiana, 47907 Email: zhao482@purdue.edu

Hongcheng Tao

School of Mechanical Engineering and Ray W. Herrick Laboratories Purdue University West Lafayette, Indiana, 47907 Email: taoh@purdue.edu

James M. Gibert*

School of Mechanical Engineering and Ray W. Herrick Laboratories Purdue University West Lafayette, Indiana, 47907 Email: jgibert@purdue.edu

ABSTRACT

A digitally encoded mechanical metamaterial utilizing selective insertion of rigid elements into an elastomeric matrix achieves programmable stiffness based on geometric patterns. Beyond the linear behavior, interests are developed towards the nonlinear stiffness region to extend the application of such metamaterials from vibration isolation to shock mitigation. A 12-unit-cell prototype is constructed and experimentally characterized under compression and drop tests, yielding the stress-strain curves and energy absorption capabilities of all independent geometric patterns identified, respectively, with validation by finite-element analysis. The versatility of the metamaterial is illustrated via a categorization of its pattern-dependent responses.

1 INTRODUCTION

Mechanical metamaterials are engineered materials whose architecture is carefully crafted to produce unconventional properties. Examples of these properties include negative Poisson's ratio [1, 2, 3, 4, 5, 6], negative thermal expansion [7, 8, 9, 10, 11], quasi-zero [12, 13, 14, 15] and negative stiffness [16, 17, 18, 19], negative effective mass [20, 21], acoustic bandgaps [22, 23], programmable mechanical behavior [24, 25, 26, 27, 28], chiral elasticity [5,29,30], and reciprocity breaking [31,32,33,34]. In many of these applications the material may be tuned prior to achieve a given constitutive relationship or desired engineering property.

This work builds upon a digitally encoded metamaterial [25] which modifies the behavior of an elastomer by inserting an elastic member with a higher modulus than the host material (Fig. 1a) or an inclusion with a higher density than the host material. Such insertions permit a spectrum of material behavior from the host structure. Fundamentally, this insert also introduces heterogeneity in the elastomer matrix and allows the material to reach a comprehensive range of tunable stiffness values. Choe et. al [35] investigated in a similar concept of metamaterial with shapememory function achieved by pixelated pattern, which is actuated with an embedded low-melting-point-alloy layer. In these designs, patterns with more proportion of pixelated activation exhibit steeper stress-strain response, implying more energy absorbed. However, the energy absorption ability of such kind of programmable stiffness metamaterial towards higher strain remains to be explored, while its potential is expected to rise as approaching the nonlinear stiffness region. This work builds upon previous research by not only investigating the tunable linear stiffness that can be achieved, but also taking into consideration the full force-displacement relationship.

2 MANUFACTURING AND ENCODING SCHEME

The metamateiral prototype consists of a 2-dimensional collapsible elastomer matrix with 12 tessellated diamond shaped holes, which is cast with degassed Smooth-On Mold Star 15 silicone rubber in a 3D-printed mold (Fig. 1a). Its mechanical

^{*}Address all correspondence to this author.

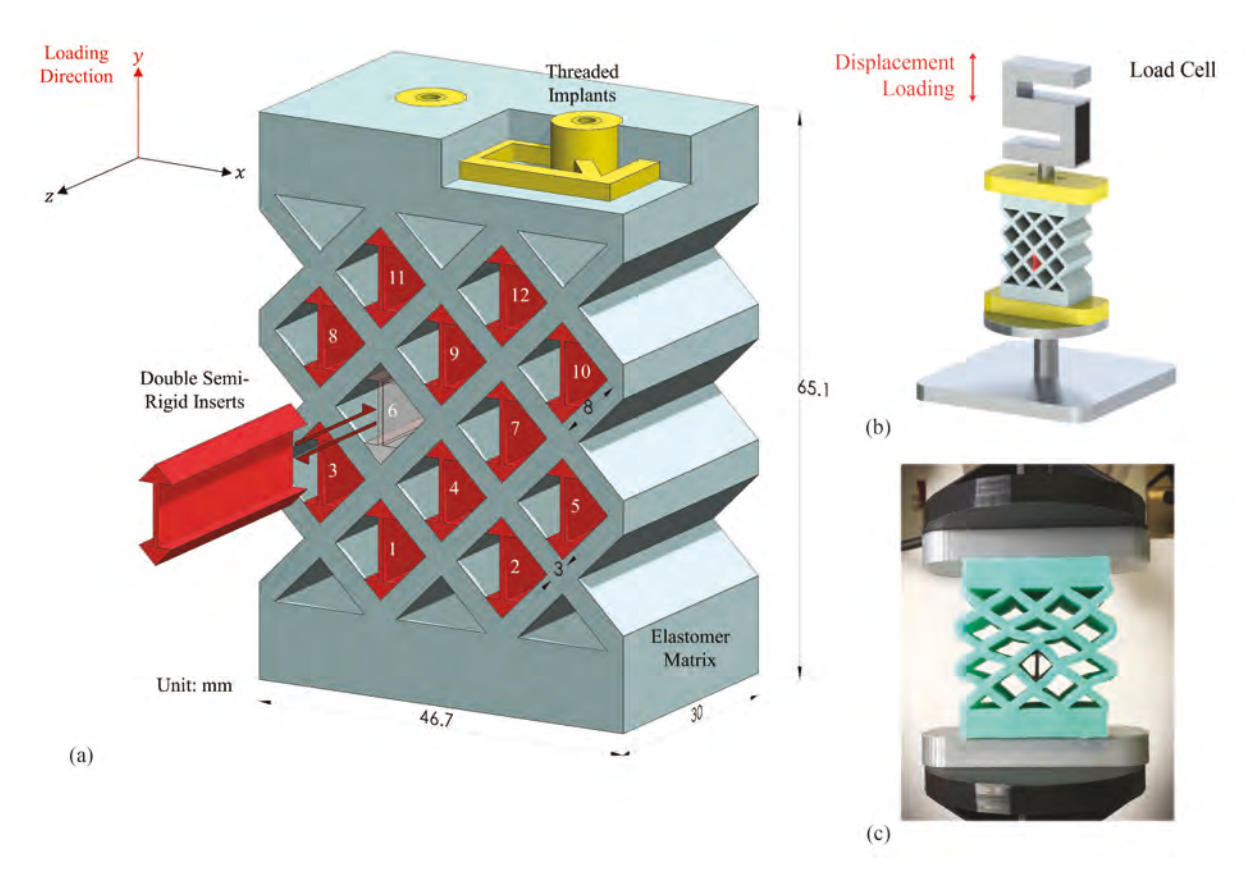


FIGURE 1: Heterogeneous programmable mechanical metamaterial: a) Dimensions of the prototype filled with longitudinal inserts enhancing compressive stiffness, where integers indicate the corresponding digit of each unit cell for pattern encoding, b) Specimen with load cell, and c) compressed metamaterial with 1 insert.

properties are programmed with semi-rigid inserts 3D-printed in PLA. Threaded implants are utilized as connectors to fixtures so that creep of unit model in tangential direction is restricted during cyclic loading test. The material may be encoded as a 12 digit binary number by using 1 and 0 to represent the presence and absence of an insert, respectively. It implies 2¹² possible force-displacement relations however by admitting only symmetric patterns the number of relationships reduces to 72.

3 EXPERIMENTAL RESULTS

To obtain empirical results, tests have been conducted on a motorized test stand (Mark-10 ESM1500) for the 72 Encoding configurations. For the test setup, elastomer matrix is screwed onto fixtures at both ends, with same reinforcement implemented between fixtures and test plates (Figure 1). After double semirigid inserts are assembled, experiments can be initiated at constant loading speed of 15 mm/min. While each configuration can be compressed to various limit, before the semi-rigid inserts are bent or flipped, due to its unique stiffness curve. These 72 config-

urations are initially classified into 6 different ranks from 0 to 5, which correspond to certain compression limits (Table 1), based on the overall vertical space occupied by double semi-rigid inserts. In addition, some configurations exhibit higher endurance limit during the tests due to their special assembly layout, and thus are reranked into the Encoding Scheme. On the other hand, certain assembly configurations may twist the elastomer matrix in a way that causes semi-rigid inserts more likely to flip, especially when they arrive at the nonlinear stiffness region, and hence not able to reach desired compression limits with respect to their ranks. Those exceptions are also summarized in Table 1 with compress limits determined.

Due to implementation of elastomer matrix, hysteresis effect exists as shown in Figure 4, and 10 continuous cycles at 15 mm/min are applied to evaluate it. Throughout the cycles, it is found that the hysteresis is consistent, as indicated in the plot, and remains similar consistency for all configurations. Meanwhile, there is noticeable Mullin's effect within the first cycle, but it quickly becomes negligible as approaching nonlinear stiffness region, or Region III in the figure, for all configurations.

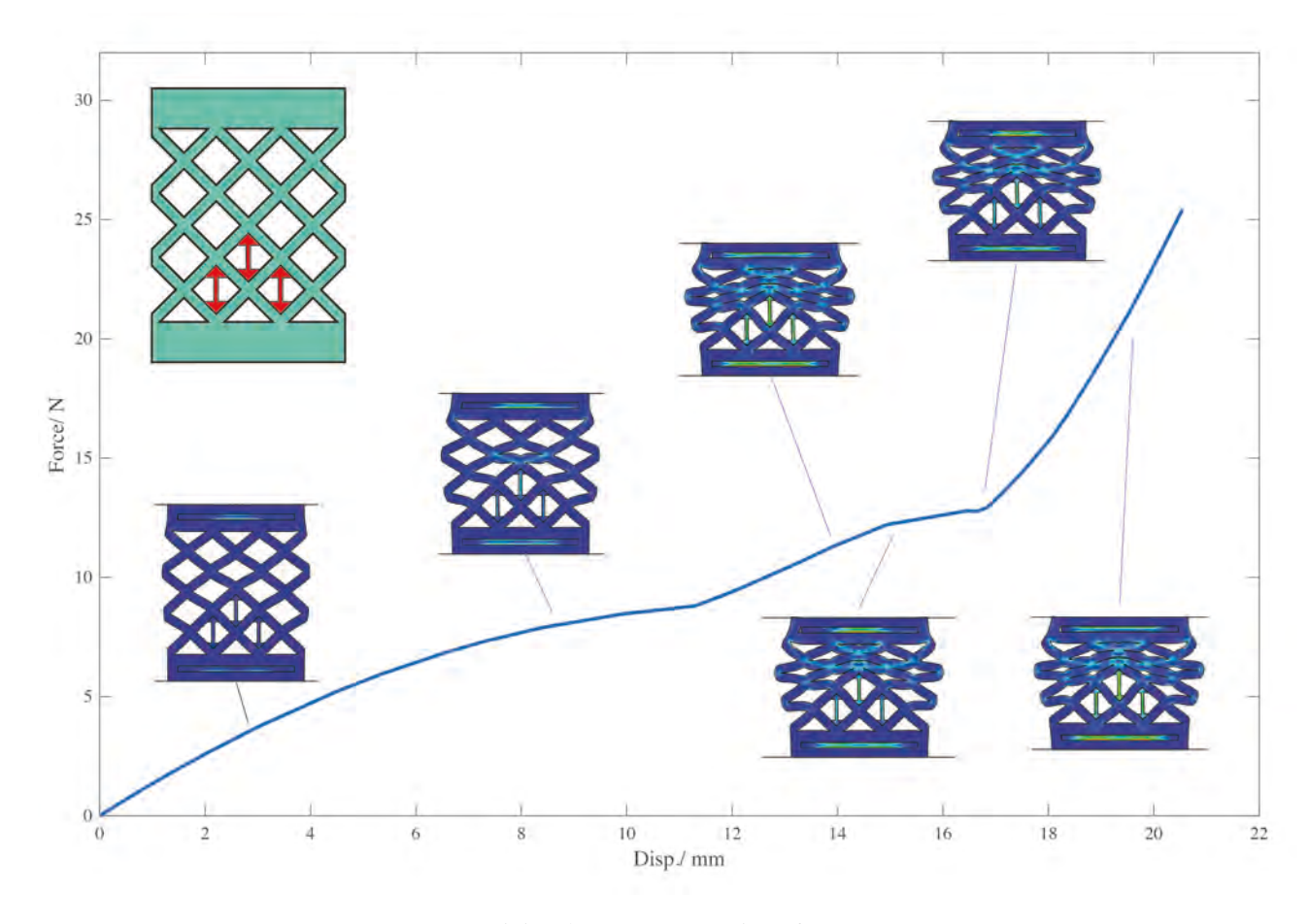


FIGURE 2: Finite element compression of 110100000000.

Therefore, the cyclic compression test is always run for at least 3 cycles for each configuration with the last loading stage to be analyzed for energy absorption ability. For the configuration (Encoding: 000001101000) illustrated as an example, it has a 3-stage stiffness response with zero and negative stiffness regions involved, and the overall response is divided into 3 regions at locations where new stage of stiffness initiated.

4 MODELING

In addition, finite element models have been established to predict the behaviors of 72 configurations identified and compare with corresponding experimental results. The models are developed in ABAQUS using Static Riks analysis with CPS3 element to deal with nonlinearity. Although they are 2D-planar models, plane stress thickness is assigned in sections, respectively, to simulate the tests and reduce computational costs significantly. For material properties of semi-rigid inserts and threaded implants, Young's Modulus of 3.1 GPa, Poisson's ratio of 0.3 and density of 1.24 g/cm³ are implemented. And previous research by

Joodaky [36] is referred to determine the material properties of elastomer matrix in finite element model, with Young's Modulus of 0.4324 MPa, Poisson's Ratio of 0.49 and density of 1.1 g/cm³. The prototype is placed between two rigid wires with surface contact, which simulate the test plates during cyclic loading test. With bottom wire to be fixed, the top wire is allowed to compress down to certain displacement limit based on the rank of configuration identified, which also serves as stopping criteria of Static Riks analysis. In addition, the whole elastomer matrix is assigned with self contact while surface contacts are set between it and semi-rigid inserts as well as threaded implants. Normal and tangential behaviors are defined for surface contact as hard contact and penalty, respectively, with friction coefficients of 0.4 between elastomer matrix and simi-rigid inserts, but 1 between elastomer matrix and wire, as well as 1 between elastomer matrix and threaded implants to prevent slipping. While self contact is accounted in tangential direction as penalty with friction coefficient of 0.6. To mimic experiments accomplished by Mark-10 ESM1500 test stand, force-displacement relationships are tracked from the top surface of finite element model through-

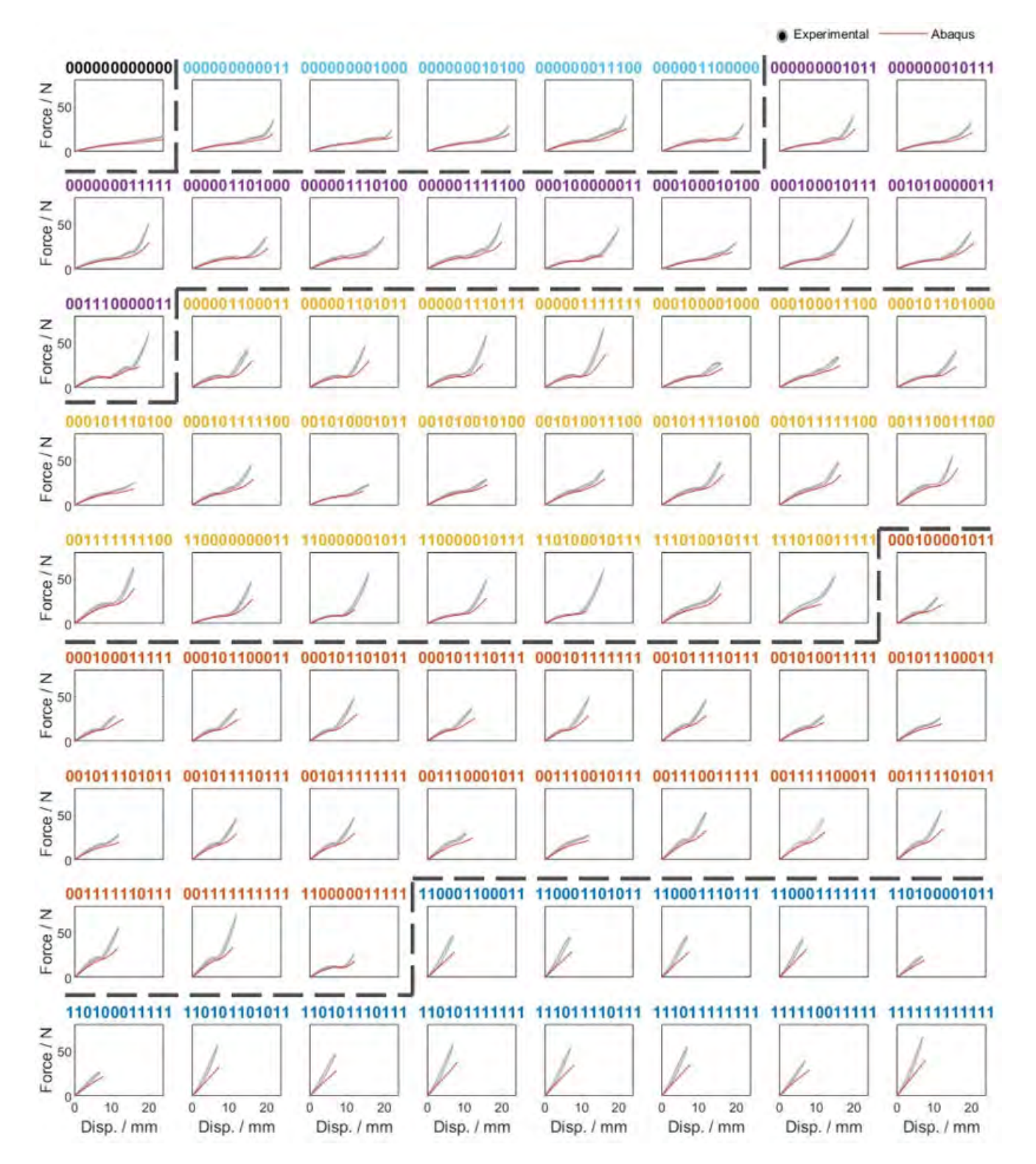


FIGURE 3: Enumeration of force displacement curve for all programmable patterns. The color coding represent the rank of the material, i.e., the row containing inserts. Rank 0, Rank 1, Rank 2, Rank 3, Rank 4, and Rank 5.



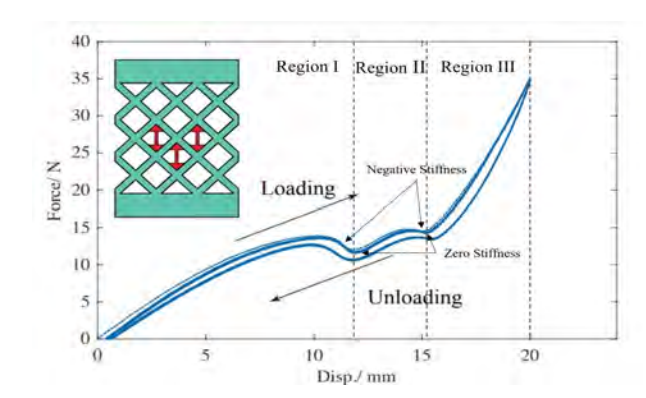


FIGURE 4: Hysterisis in specimens

| Rank | Compression Limit (mm) | Encoding | Test Limit (mm) |
|------|---------------------------|--|-----------------------|
| 0 | 28 | No Failure | No Failure |
| 1 | 22 | No Failure | No Failure |
| 2 | 20 | No Failure | No Failure |
| 3 | 16 | 001110011100 111010011111 000001100011 | 15 15 15 15 |
| 4 | 12 | 001110001011 000100001011 000100011111 | 10.5 11 11 |
| 5 | 7 | 110001111111 | 6.5 |

TABLE 1: Configurations that fail to reach corresponding compression limits due to special assembly layouts.

out the simulation. It should be noted that initial arc length increment may need to be adjusted for certain configurations to properly initiate simulations.

5 RESULTS

Table 2 indicates the maximum strain, plateau stress, toughness, nonlinear region toughness and its percentage of configurations in each rank. As expected, larger maximum strain can be achieved with configurations at lower ranks. Meanwhile, although plateau stress also generally rises as rank elevates, its presence primarily depends on the configuration. For example, the one that is filled with inserts (Encoding: 1111111111111) and the one without any inserts (Encoding: 0000000000000) do not

| Rank | Max. Strain | Plateau Stress (Pa) | $\begin{array}{c} \textbf{Toughness} \\ (\textbf{J/m}^3) \end{array}$ | Nonlinear Region Toughness (J/m³) | Nonlinear Region Toughness Proportion (%) 15.71 31.52 42.77 66.05 69.46 |
|------|----------------|---------------------------|---|--|--|
| 0 | 0.4301 | - | 3283.2 | 515.9 | 15.71 |
| 1 | 0.3379 | 6923.6 | 2713.9 | 855.5 | 31.52 |
| 2 | 0.3072 | 8993.6 | 3353.2 | 1434.3 | 42.77 |
| 3 | 0.2458 | 10278.4 | 3399.0 | 2244.9 | 66.05 |
| 4 | 0.1843 | 15845.8 | 3488.0 | 2422.7 | 69.46 |
| 5 | 0.1075 | - | 2291.8 | - | - |

have plateau region and therefore no plateau stress. As for toughness, higher rank implies higher energy absorption ability except rank 0 and 5, where rank 0 has no inserts and thus can be compressed for about 27% more than rank 1 to absorb more energy. And rank 5 configurations are generally filled with too many inserts for them to be compressed at a similar level to previous ranks, or even initiate another stage of stiffness region before inserts are bent or flipped. However, nonlinear region toughness insistently increases with its proportion rises from 15.71% at rank 0 to 69.49% at rank 4, which implies that the nonlinear stiffness region can contribute significantly for energy absorption. The loading process of each configuration has also been simulated in Abaqus, which exhibits a similar stress-strain relationship with corresponding multiple-stage stiffness regions, and the collapse of elastomer matrix matches experimental observation.

Drop tests are performed to investigate the deformation of prototype upon impact using a high-speed camera. As indicated in the figures, a 2-inch Chrome Steel ball weighing 534.46g is dropped on two different configurations (Encoding: 000001100000, 000001101000) from 0.1m, 0.2m and 0.3m, respectively. And the markers on the prototype are tracked using ImageJ and TrackMate while the resolution of high-speed camera is set at maximum (1920x1280) with 1000 frame per second. Upon impact, the marker tracked, which is right below the point of contact, quickly reaches the free drop velocity of the ball with respect to its drop height and stays at similar level of speed for around 0.01 second before the sample is collapsed into nonlinear stiffness region. Overall, the finite element models properly simulate drop tests and further indicate the energy absorption ability of nonlinear stiffness region.

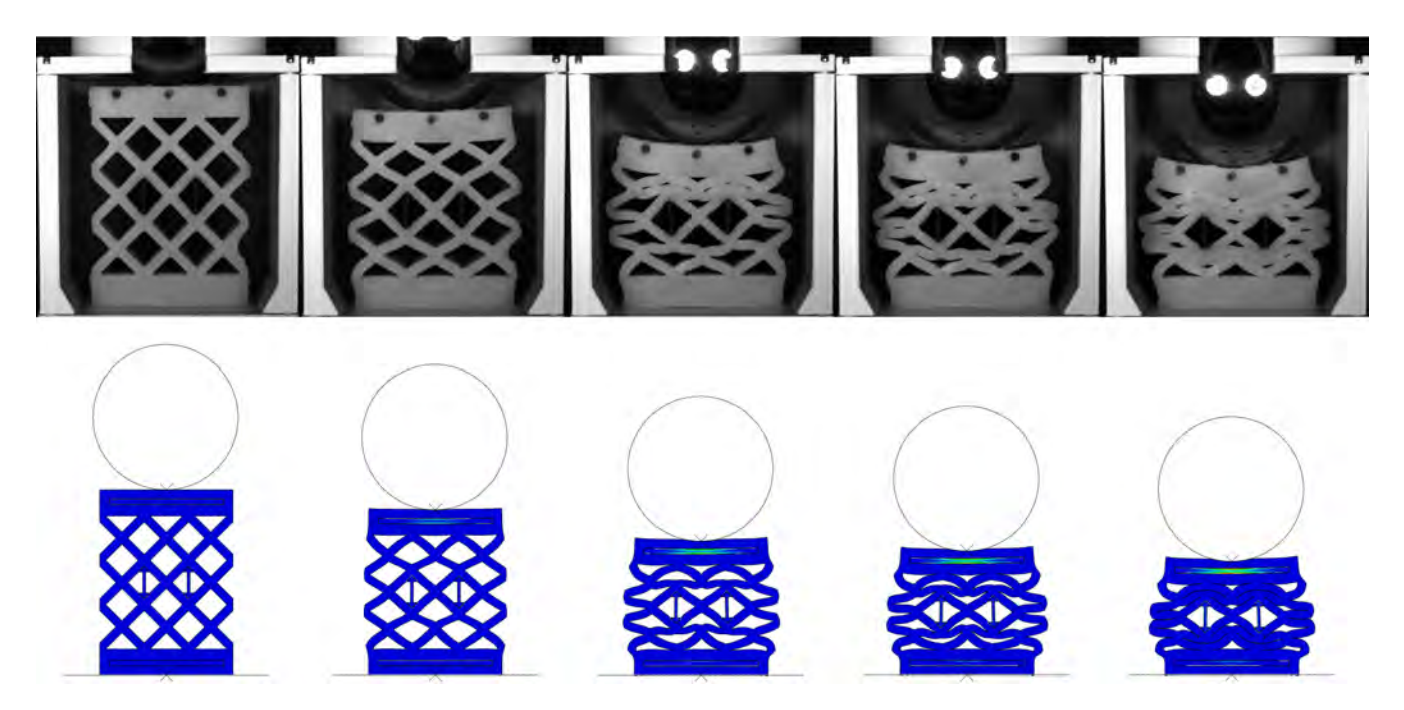


FIGURE 5: Comparison on deformation from 0.1m impact between physical test and finite element simulation (Encoding: 000001100000)

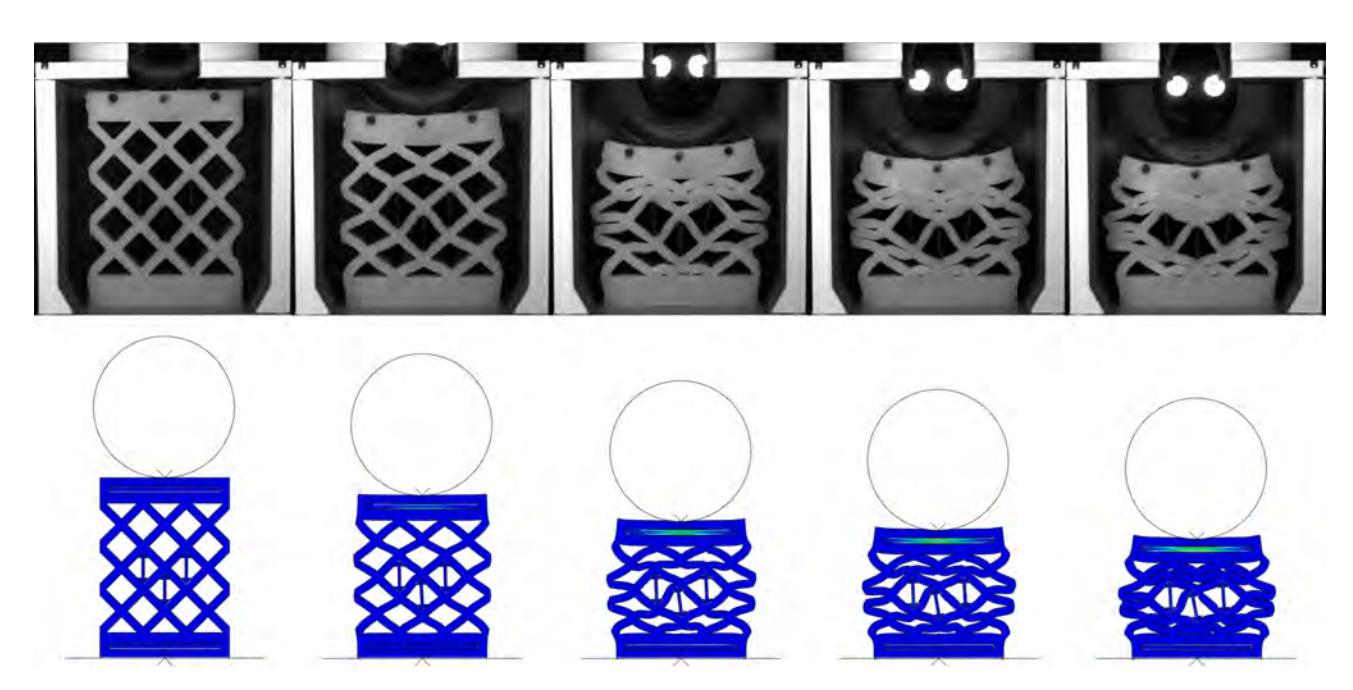


FIGURE 6: Comparison on deformation from 0.1m impact between physical test and finite element simulation (Encoding: 000001101000)

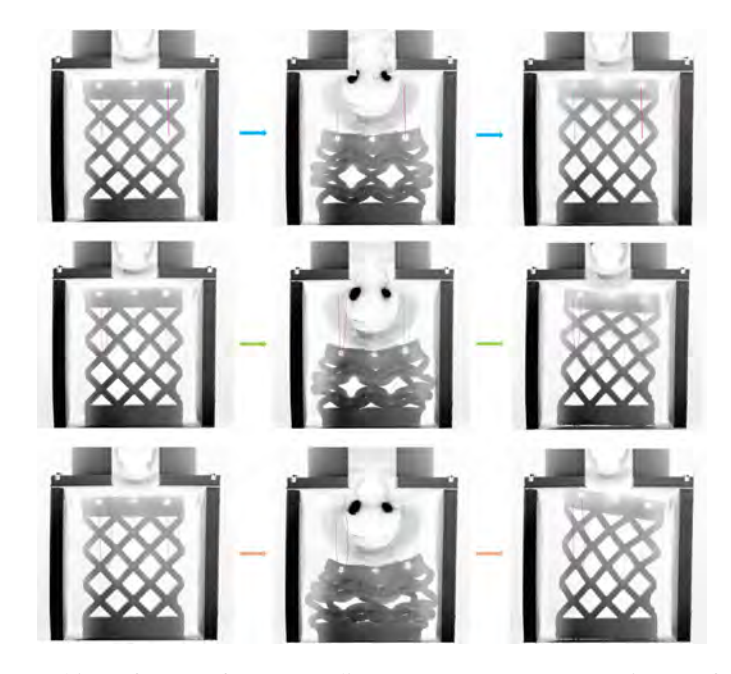


FIGURE 7: Displacement tracking of top surface (Encoding: 000001100000) upon impact from 0.1m, 0.2m and 0.3m.

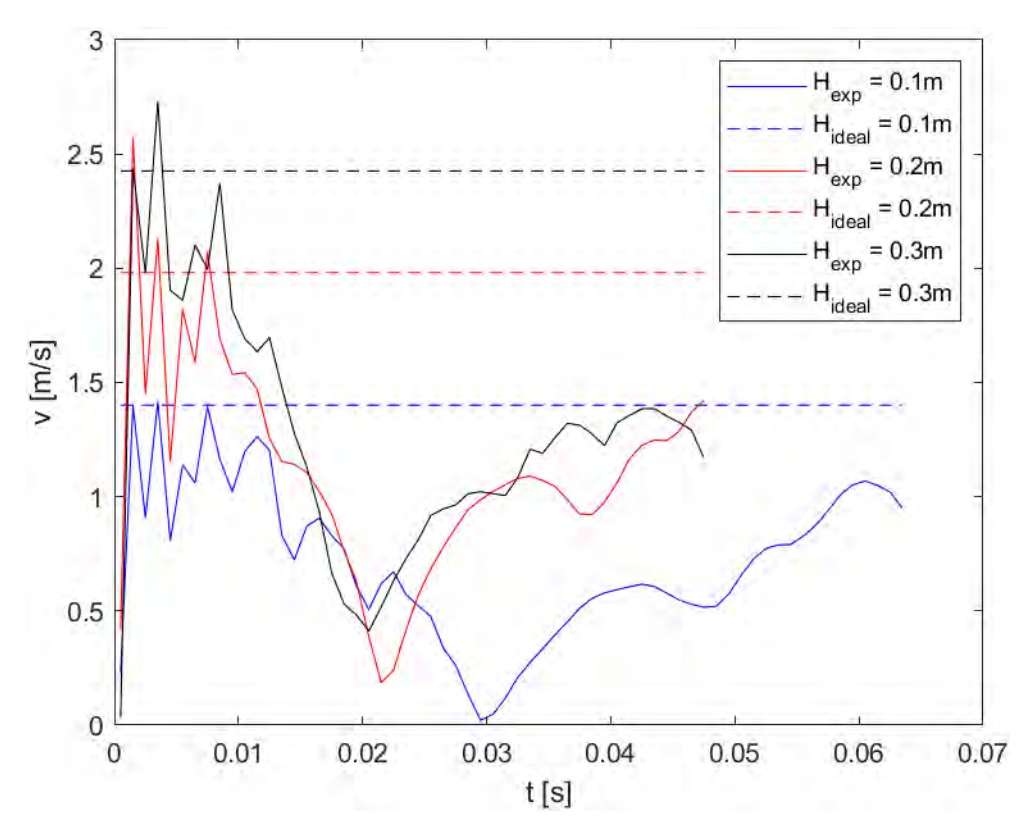


FIGURE 8: Comparison of velocities on top surface of protorype (Encoding: 000001100000) upon impact from different heights, as well as the ideal drop velocities of striker from these altitudes

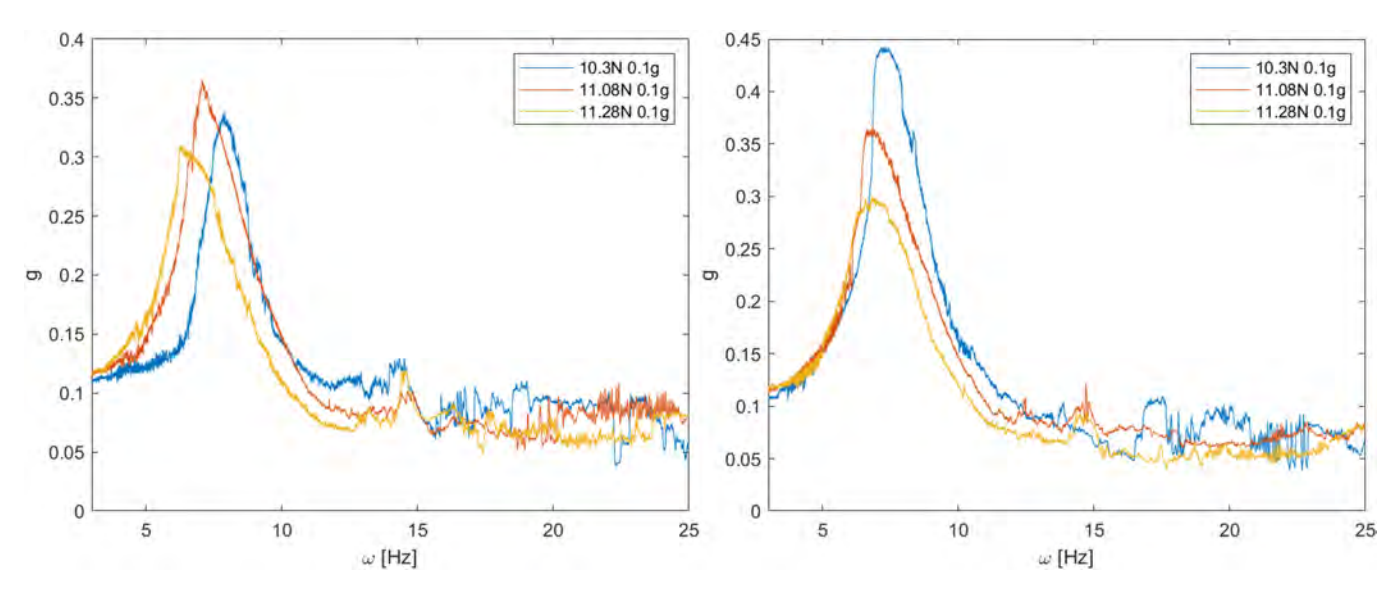


FIGURE 9: Excitation at 0.1g as frequency increasing (left) and decreasing (right). The loadings are identified to be the ones near the peak on load-displacement plot, implying a change from positive stiffness to negative stiffness region. (Encoding: 001110000011)

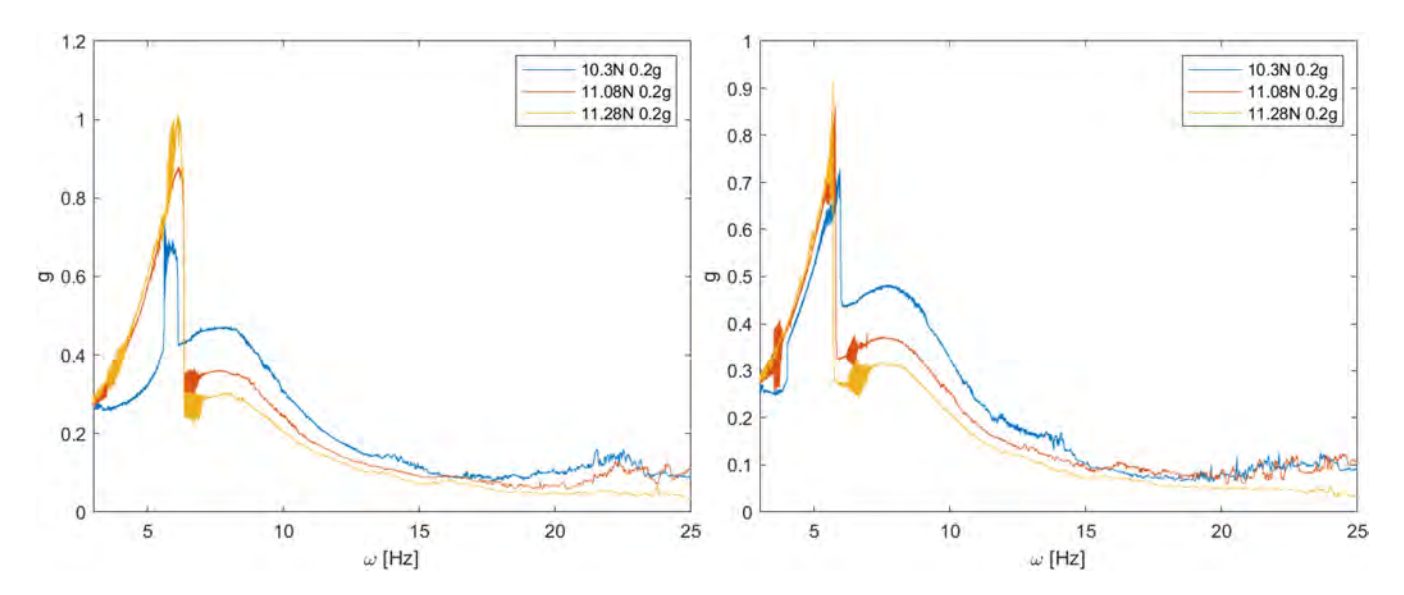


FIGURE 10: Excitation at **0.2***g* as frequency increasing (left) and decreasing (right). The loadings are identified to be the ones near the peak on load-displacement plot, and the sudden jump indicates that matrices are buckled to another bistable state at higher excitation acceleration. (Encoding: 001110000011)

In addition, shaker tests are also implemented to explore low frequency impact. The chosen model (Encoding: 001110000011) has negative stiffness region, which implies that a same compression displacement can be reached at different forces applied. Therefore, the shaker tests are initiated at bistable states with weight of 10.3N and 11.28N, as well as a third weight of 11.08N to investigate the transition from positive stiffness to negative stiffness. As can be observed, the sample with heavier weight applied tends to have lower natural frequency when excited at **0.1**g. In other words, the natural frequency of the programming stiffness model is "softened" by extra weight applied. Besides, sudden jump can be observed when it is excited at **0.2**g, which is simply too drastic for this model at current size and causes the elastomer matrix to be buckled into another bistable state.

6 CONCLUSIONS

As both experiments and simulations indicated, there is huge potential at nonlinear stiffness region of the digital mechanical metamaterial for energy absorption. And as the rank rises, although the maximum strain that can be reached drops noticeably, the energy absorption ability can still be improved with major contribution from the nonlinear stiffness region. And such nonlinear region toughness contribution at rank 4 is more than 4 times **than** that of rank 0, which is from a solely elastomeric matrix without any enhancing elements. Furthermore, such a programming stiffness elastomer matrix can be easily expanded to a variety of sizes and the corresponding nonlinear region toughness contribution is expected to dominate its energy absorption ability for any higher ranks.

ACKNOWLEDGMENT

The authors would like to acknowledge the financial support provided by NSF CAREER Award: CMMI 2145803.

REFERENCES

- [1] Lakes, Roderic. "Foam Structures with a Negative Poisson's Ratio." *Science* Vol. 235 No. 4792 (1987): pp. 1038–1040. doi:10.1126/science.235.4792.1038.
- [2] Evans, K E. "Tensile network microstructures exhibiting negative Poisson's ratios." *Journal of Physics D: Applied Physics* Vol. 22 No. 12 (1989): p. 1870. doi:10.1088/0022-3727/22/12/011.
- [3] Lakes, Roderic. "Advances in negative Poisson's ratio materials." *Advanced Materials* Vol. 5 No. 4 (1993): pp. 293–296. doi:https://doi.org/10.1002/adma.19930050416.
- [4] Bertoldi, Katia, Reis, Pedro M., Willshaw, Stephen and Mullin, Tom. "Negative Poisson's Ratio Behavior Induced by an Elastic Instability." *Advanced*

- *Materials* Vol. 22 No. 3 (2010): pp. 361–366. doi:https://doi.org/10.1002/adma.200901956.
- [5] Wenwang, Wu., Hu, Wenxia, Qian, Guian, Liao, Haitao, Xu, Xiaoying and Berto, Filippo. "Mechanical design and multifunctional applications of chiral mechanical metamaterials: A review." *Materials & Design* Vol. 180 (2019): p. 107950. doi:https://doi.org/10.1016/j.matdes.2019.107950.
- [6] Hui, Chen and Fanchun, Li. "Design, simulation and experimental verification of novel 3D metamaterial structures with negative Poisson's ratio." *Mechanics of Advanced Materials and Structures* Vol. 30 No. 1 (2023): pp. 17–28. doi:10.1080/15376494.2021.2006839.
- [7] Korthuis, V, Khosrovani, N, Sleight, AW, Roberts, N, Dupree, R and Warren, WW Jr. "Negative thermal expansion and phase transitions in the ZrV2-xPxO7 series." *Chemistry of materials* Vol. 7 No. 2 (1995): pp. 412–417.
- [8] Sleight, AW. "Thermal contraction." *Endeavour* Vol. 19 No. 2 (1995): pp. 64–68.
- [9] Jefferson, George, Parthasarathy, Triplicane A. and Kerans, Ronald J. "Tailorable thermal expansion hybrid structures." *International Journal of Solids and Structures* Vol. 46 No. 11 (2009): pp. 2372–2387. doi:https://doi.org/10.1016/j.ijsolstr.2009.01.023.
- [10] Yu, Huabin, Wang, Haomiao, Liang, Bo and Guo, Xiaogang. "Metamaterials with remarkable thermal–mechanical stability and high specific modulus: Mechanical designs, theoretical predictions and experimental demonstrations." *Extreme Mechanics Letters* Vol. 49 (2021): p. 101436. doi:https://doi.org/10.1016/j.eml.2021.101436.
- [11] Xu, Hang and Pasini, Damiano. "Structurally Efficient Three-dimensional Metamaterials with Controllable Thermal Expansion." *Scientific Reports* Vol. 6 No. 1 (2016): p. 34924. doi:10.1038/srep34924.
- [12] Zhang, Quan, Guo, Dengke and Hu, Gengkai. "Tailored Mechanical Metamaterials with Programmable Quasi-Zero-Stiffness Features for Full-Band Vibration Isolation." Advanced Functional Materials Vol. 31 No. 33 (2021): p. 2101428. doi:https://doi.org/10.1002/adfm.202101428.
- [13] Lu, Hongjie, Meng, Lixin, Wang, Jinkai, Wang, Yan and Zhang, Lizhong. "Design and Performance Study of Metamaterial with Quasi-zero Stiffness Characteristics Based on Human Body Structure." *Journal of Vibration Engineering & Technologies* doi:10.1007/s42417-023-00864-1.
- [14] Lin, Qida, Zhou, Jiaxi, Wang, Kai, Xu, Daolin, Wen, Guilin and Wang, Qiang. "Three-dimensional quasi-zero-stiffness metamaterial for low-frequency and wide complete band gap." *Composite Structures* Vol. 307 (2023): p. 116656. doi:https://doi.org/10.1016/j.compstruct.2022.116656.
- [15] Kastner, Jared, Joodaky, Amin and Gibert, James. "The Effectiveness of 2D Unit Cells in Creating χ-Spring Based Metamaterials." *Smart Materials, Adaptive Structures and Intelligent Systems*, Vol. 85499: p. V001T07A014. 2021.

- American Society of Mechanical Engineers.
- [16] Thompson, J. M. T. "Paradoxical' mechanics under fluid flow." *Nature* Vol. 296 No. 5853 (1982): pp. 135–137. doi:10.1038/296135a0.
- [17] Zhu, Shaowei, Tan, Xiaojun, Chen, Shuai, Wang, Bing, Ma, Li and Wu, Linzhi. "Quasi-All-Directional Negative Stiffness Metamaterials Based on Negative Rotation Stiffness Elements." *Physica Status Solidi (b)* Vol. 257 No. 6 (2020): p. 1900538. doi:https://doi.org/10.1002/pssb.201900538.
- [18] Tan, Xiaojun, Li, Yifeng, Wang, Lianchao, Yao, Kaili, Ji, Qingxiang, Wang, Bing, Laude, Vincent and Kadic, Muamer. "Bioinspired Flexible and Programmable Negative Stiffness Mechanical Metamaterials." Advanced Intelligent Systems (2023): p. 2200400doi:https://doi.org/10.1002/aisy.202200400.
- [19] Xiao, Lei, Bursi, Oreste S., Wang, Meng, Nagarajaiah, Satish, Sun, Feifei and Du, Xiu-Li. "Metamaterial beams with negative stiffness absorbers and rotation: band-gap behavior and band-gap merging." *Engineering Structures* Vol. 280 (2023): p. 115702. doi:https://doi.org/10.1016/j.engstruct.2023.115702.
- [20] Beli, Danilo, Fabro, Adriano T., Ruzzene, Massimo and Arruda, José Roberto F. "Wave attenuation and trapping in 3D printed cantilever-in-mass metamaterials with spatially correlated variability." *Scientific Reports* Vol. 9 No. 1 (2019): p. 5617. doi:10.1038/s41598-019-41999-0.
- [21] Liu, X. N., Hu, G. K., Huang, G. L. and Sun, C. T. "An elastic metamaterial with simultaneously negative mass density and bulk modulus." *Applied Physics Letters* Vol. 98 No. 25 (2011): p. 251907. doi:10.1063/1.3597651.
- [22] Elmadih, Waiel, Chronopoulos, Dimitrios and Zhu, Jian. "Metamaterials for simultaneous acoustic and elastic bandgaps." *Scientific Reports* Vol. 11 No. 1 (2021): p. 14635. doi:10.1038/s41598-021-94053-3.
- [23] Fang, Xin, Wen, Jihong, Bonello, Bernard, Yin, Jianfei and Yu, Dianlong. "Ultra-low and ultra-broad-band nonlinear acoustic metamaterials." *Nature Communications* Vol. 8 No. 1 (2017): p. 1288. doi:10.1038/s41467-017-00671-9.
- [24] Pan, Fei, Li, Yilun, Li, Zhaoyu, Yang, Jialing, Liu, Bin and Chen, Yuli. "3D Pixel Mechanical Metamaterials." *Advanced Materials* Vol. 31 No. 25 (2019): p. 1900548. doi:https://doi.org/10.1002/adma.201900548.
- [25] Tao, Hongcheng, Danzi, Francesco, Silva, Christian E and Gibert, James M. "Heterogeneous digital stiffness programming." Extreme Mechanics Letters Vol. 55 (2022): p. 101832.
- [26] Fang, Xin, Wen, Jihong, Cheng, Li, Yu, Dianlong, Zhang, Hongjia and Gumbsch, Peter. "Programmable gear-based mechanical metamaterials." *Nature Materials* Vol. 21 No. 8 (2022): pp. 869–876. doi:10.1038/s41563-022-01269-3.
- [27] Chen, Tian, Pauly, Mark and Reis, Pedro M. "A reprogrammable mechanical metamaterial with stable mem-

- ory." *Nature* Vol. 589 No. 7842 (2021): pp. 386–390. doi:10.1038/s41586-020-03123-5.
- [28] Trainiti, Giuseppe, Xia, Yiwei, Marconi, Jacopo, Cazzulani, Gabriele, Erturk, Alper and Ruzzene, Massimo. "Time-Periodic Stiffness Modulation in Elastic Metamaterials for Selective Wave Filtering: Theory and Experiment." *Phys. Rev. Lett.* Vol. 122 (2019): p. 124301. doi:10.1103/PhysRevLett.122.124301.
- [29] Prall, D. and Lakes, R.S. "Properties of a chiral honeycomb with a poisson's ratio of 1." *International Journal of Mechanical Sciences* Vol. 39 No. 3 (1997): pp. 305–314. doi:https://doi.org/10.1016/S0020-7403(96)00025-2. URL https://www.sciencedirect.com/science/article/pii/S0020740396000252.
- [30] Runkel, Falk, Molinari, Giulio, Arrieta, Andres F. and Ermanni, Paolo. "Novel Chiral Structure With Tailored Mechanical Response Exploiting Elastic Instabilities." Vol. Volume 2: Modeling, Simulation and Control; Bio-Inspired Smart Materials and Systems; Energy Harvesting. 2016. doi:10.1115/SMASIS2016-9162.
- [31] Coulais, Corentin, Sounas, Dimitrios and Alù, Andrea. "Static non-reciprocity in mechanical metamaterials." *Nature* Vol. 542 No. 7642 (2017): pp. 461–464. doi:10.1038/nature21044.
- [32] Bertoldi, Katia, Vitelli, Vincenzo, Christensen, Johan and van Hecke, Martin. "Flexible mechanical metamaterials." *Nature Reviews Materials* Vol. 2 No. 11 (2017): p. 17066. doi:10.1038/natreymats.2017.66.
- [33] Brandenbourger, Martin, Locsin, Xander, Lerner, Edan and Coulais, Corentin. "Non-reciprocal robotic metamaterials." *Nature Communications* Vol. 10 No. 1 (2019): p. 4608. doi:10.1038/s41467-019-12599-3.
- [34] Trainiti, G and Ruzzene, M. "Non-reciprocal elastic wave propagation in spatiotemporal periodic structures." *New Journal of Physics* Vol. 18 No. 8 (2016): p. 083047. doi:10.1088/1367-2630/18/8/083047.
- [35] Choe, Jang Won Lee Lee Jang Song, Yi and Kim, Jiyun. "Digital Mechanical Metamaterial: Encoding mechanical information with graphical stiffness pattern for adaptive soft machines." *Advanced Materials* Vol. 36. doi:10.1002/adma.202304302.
- [36] Joodaky, Amin. "Mechanics and Design of Polymeric Metamaterial Structures for Shock Absorption Applications." Ph.D. Thesis, Purdue University Graduate School. 2020.